Grain-Size Effects in the Quasi-Static Fracture Resistance of a Thermally Embrittled RPV Steel (Quenched and Tempered Microstructures)

J.R. Tarpani, W.W. Bose Filho, and D. Spinelli

(Submitted 19 March 2002)

The elastic-plastic fracture toughness and crack extension behavior under the quasi-static loading regimen of several thermally embrittled conditions of a nuclear reactor pressure vessel (RPV) steel were assessed on the basis of microstructural parameters. It was discovered that the bainite packet size is the fracture properties controlling parameter of single-phase quenched and tempered microstructures. Results were found in close agreement to those obtained in a parallel study with dual-phase annealed microstructures derived from the same low alloy steel. Similarly, it was concluded that a Hall-Petch type relationship correlates J-fracture mechanics criteria to the grain size.

Keywords fracture toughness, Hall-Petch relationship, J-R curve, neutron damage simulation, RPV steel

1. Introduction

In a previous work,[1] a nuclear-grade steel was submitted to annealing heat treatments that were devised to obtain a variety of low elastic-plastic fracture toughness in the quasi-static loading regimen. Thermal cycles were designed to simulate the mechanical behavior of damaged structural steels undergoing high neutron doses in radioactive environments, e.g., reactor pressure vessel (RPV) steels. By means of a simple rule of mixture, it was concluded that the equivalent grain size of the dual-phase annealed microstructures was the parameter controlling overall fracture properties. The procedure was based on the relative percentage of both phases present in the heat-treated alloy, similar to that applied in the inference of mechanical properties of composite materials. Nonetheless, it became clear that despite the broad range of fracture toughness so achieved, the annealing heat treatments did not generate microstructures with hardness and tensile properties, that is, yield and ultimate tensile strengths closely comparable with neutron-damaged low-alloy structural steels. For instance, an increase in yield strength up to 150 MPa has been reported for RPV steels in the early life stages of commercial nuclear power plants.[2,3] However, just a fraction of this value has been achieved even for the severest annealing heat treatment.[1] Therefore, alternative quenching and tempering (Q&T) routes were designed and applied to the original A508 steel to produce additional embrittled microstructures that minimally satisfied those mechanical requirements.

J.R. Tarpani, W.W. Bose Filho, and **D. Spinelli,** Materials, Aeronautical and Automotive Engineering Department-SMM, Engineering School of São Carlos-EESC, University of São Paulo-USP, Av. Trabalhador São-Carlense, 400, São Carlos-SP, 13566-590-Brazil. Contact e-mail: jrpan@sc.usp.br.

2. Base Material

The Brazilian ASTM A508 Class 3A steel is a typical RPV material designed for the nuclear industry whose original heat treatment and globular bainite microstructure (8.5 ASTM grain size number) are fully described elsewhere.[1]

3. Experimental and Analytical Procedures

3.1 Quenching and Tempering Thermal Cycles

Figure 1 shows schematic drawings for the six embrittling heat treatments, named from I to N, which were individually applied to the A508 steel in the as-received condition.

3.2 Mechanical Properties and Fracture Toughness Test

Hardness measurements at ambient temperature and tensile tests at 300 °C were performed for the Q&T-embrittled materials.

Performed likewise with the annealed and as-delivered states of the A508 steel,[1] fracture mechanics J-R curve testing was performed via the unloading elastic compliance (UEC) technique. Subsized 5 mm and 10 mm thick compact tensile specimens, 0.2 T and 0.4 T C [T], side-grooved (SG) to 20% and 33% of their gross-thickness B_G, were loaded at 300 °C and a cross-head speed of 0.3 mm/min. Procedures were identical as followed in the literature[1] concerning the tasks for J-Δa data points determination, data fitting and extrapolation, as well as for deriving the initiation J value, J_i, the Paris & Johnson criterion, J_{50}, and the increase rate on J-crack growth resistance at 1 mm of crack extension, $dJ_D/d\Delta a_{(1mm)}$. As a general rule, three test pieces were tested for each condition so that J_i, J_{50}, and $dJ_D/d\Delta a_{(1\ mm)}$ results provided herein always refer to the mean values.

4. Results and Discussion

4.1 Microstructural Characterization

Shown in Fig. 2 is the microstructure I, which is essentially composed of low carbon (C) martensite packets, slightly de-

composed in ferrite and carbides as a result of mild tempering. The largest austenite grain size obtained among all the Q&T microstructures gave rise to the highest steel hardenability state, which favored martensite transformation and retention of austenite on quenching, the latter as small acicular areas. Partial recrystallization of the alloy during discontinuous cooling may have induced a wide distribution of austenite grain sizes, whereas elevated austenitizing temperatures provided, not to mention the very coarse microstructure, alloying segregation at the grain boundaries. This segregation, identified mainly as Mn and C by dispersed x-ray microanalyses, was probably the chief cause for the intergranular fracture mode observed in this microstructure during quasi-static fracture toughness testing.

Nomenclature

a, b, c, d, e, f	fitting constants
A, I, J, K, L, M, N	microstructure nomination
AC	air cooling
ASTM	American Society for Testing and Materials
B_G	gross thickness (mm)
BHN	Brinell hardness number
C[T]	compact tensile specimen
$dJ_{(D)}/d\Delta a$	increase rate on J-crack growth resistance ($kJ/m^2/mm$)
$D_{bainite(martensite)}$	mean diameter of tempered bainite (martensite) packet (μm)
D_0	original diameter (mm)
EGS	equivalent grain size (μm)
FC	furnace cooling
J	J-integral (kJ/m^2)
J_D	deformation-J (kJ/m^2)
J_i (J_{IC})	initiation J (plane-strain) (kJ/m^2)
J-R	J-crack resistance curve
J_{50}	Paris and Johnson criterion (kJ/m^2)
L_0	original gage length (mm)
m	coefficient of power-law stress-strain relationship (MPa)
n	exponent of power-law stress-strain relationship
OQ	oil quenching
PWHT	postwelding heat treatment
Q&T	quenching and tempering
R	coefficient of correlation
RA	reduction in area at fracture (%)
RCS	representative cell size (μm)
RPV	reactor pressure vessel
SG	side-groove level (%)
S_U	ultimate tensile strength (MPa)
S_Y	yield strength (MPa)
T	specimen thickness (in.)
UEC	unloading elastic compliance
WQ	water quenching
Δa	ductile crack growth (mm)
ε	nominal strain (%)
σ	nominal stress (MPa)

Microstructure J presented heavily spheroidized carbides, as a result of hard tempering. Steel hardenability was reduced because of the three recrystallization, grain homogenization, and refinement thermal cycles, sequentially applied to the material, which favored bainite transformation and prevented austenite retaining.

Microstructure K exhibited a quite complex arrangement of several phases, in which it was found to retain austenite, tempered martensite, and bainite, as well as a mixture of ferrite and carbides slightly coalesced on tempering process. This unique microstructure experienced catastrophic cleavage in both tensile and fracture toughness testing, possibly as a result of the considerable amount of retained austenite.

Microstructure L exhibited some morphologic similarity with J microstructure, probably owing to the likeness between their quenching and final tempering conditions. However, as a consequence of higher austenitizing soaking time and temperature, comparatively to J, as well as the absence of grain refinement and homogenization thermal cycles, a coarser microstructure was obtained. This led to a lower elastic-plastic fracture toughness performance for microstructure L if compared with J, as verified by the respective J-R curves.

Correspondingly, microstructure M showed a great similarity with microstructure I in terms of grain coarseness and the nature of the essential microconstituent, typical low C martensite. This microstructure also presented alloying segregation at the grain boundaries and intergranular crack propagation during fracture toughness testing.

Also in Fig. 2 is the microstructure N, which underwent the same Q&T thermal cycles applied during fabrication of the original A508 steel (code A[1]), except by the subsequent postwelding heat treatment (PWHT). Comparing with microstructure A, shorter soaking times were used to produce microstructure N to offset the huge in-scale differences between heat treated samples; relatively small blankets for N against thick-section plate for A. This procedure allowed for the achievement of similar tempered bainite packet size and led microstructure N to exhibit a reasonably comparable performance than A.

Table 1 supplies bainite and martensite packet sizes of the materials tested. Hardenability is shown to be a function of previous austenite grain size where martensite derives from the largest grain sizes, whereas bainite is always produced from intermediate and fine- grained materials.

4.2 Hardness and Tensile Properties

Table 2 lists conventional mechanical properties of the materials tested. It can be noticed that hardness BHN, yield S_Y, and ultimate S_U, tensile strengths of the Q&T products are substantially higher than those found for the A508 steel in both as-delivered and annealed conditions.[1] Therefore, Q&T heat treatments seem to be potentially more efficient than annealing to simulate hardening and strengthening effects typically developed in nuclear grade steels due to neutron irradiation damage.

Figure 3 displays the tensile flow curves of the materials till the maximum load capacity, according to the following power-law behavior model:

$$\sigma = m \cdot \varepsilon^n \quad \text{(Eq 1)}$$

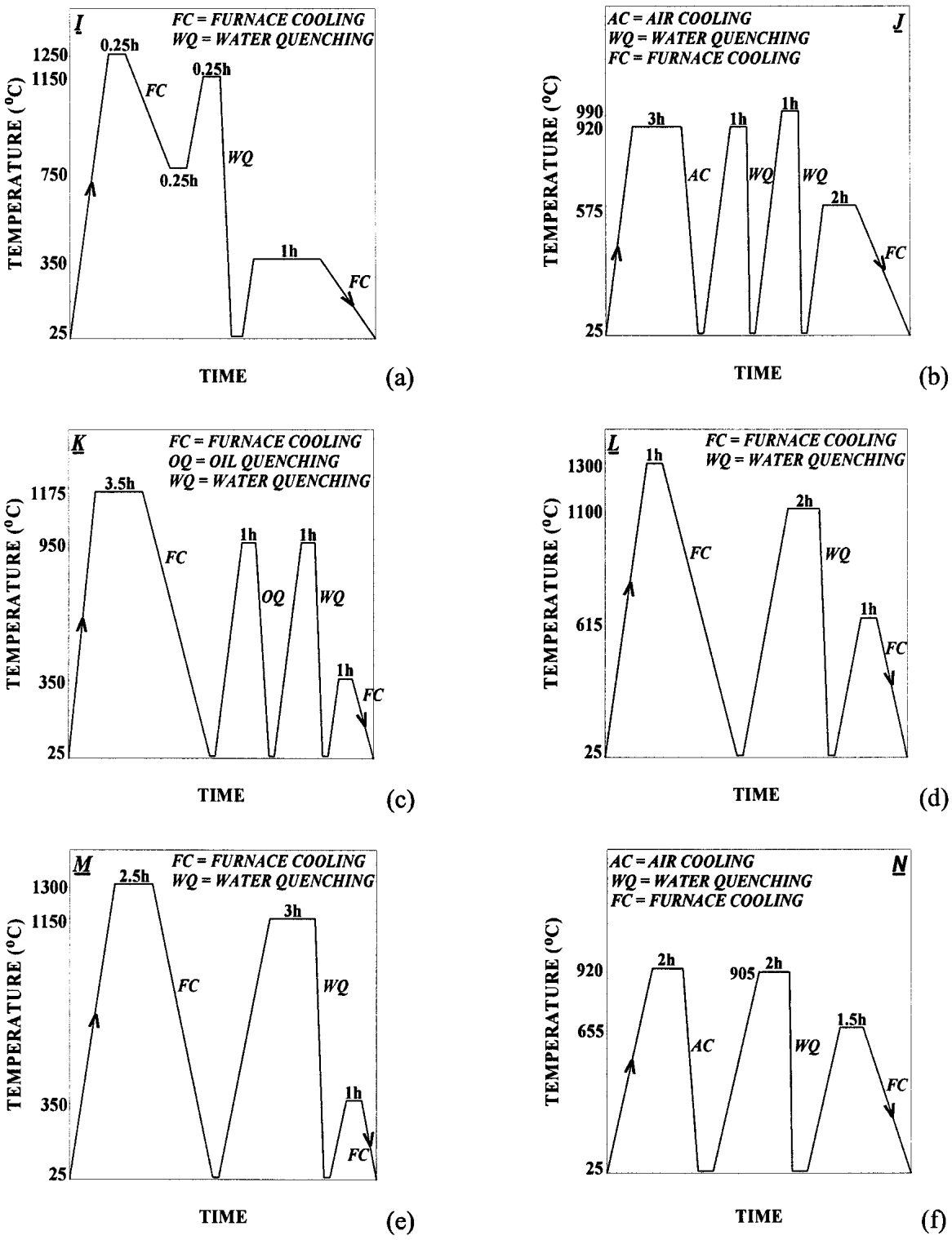

Fig. 1 Schematic drawings of Q&T routes individually applied to the original A508 steel (A) to generate thermally embrittled microstructures: **(a)** I, **(b)** J, **(c)** K, **(d)** L, **(e)** M, and **(f)** N

where σ and ε are respectively the nominal stress and strain, and m and n are fitting constants, the latter supplied in Table 2.

Figure 3 proves that, as a general rule, Q&T microstructures are stronger than annealed ones. To some extent, the very high yield and ultimate strengths exhibited by microstructures I, K, and M are related to the intergranular brittle fracture mode developed in microstructures I and M during J-R curve testing, and the cleavage rupture mode in microstructure K. It is inter-

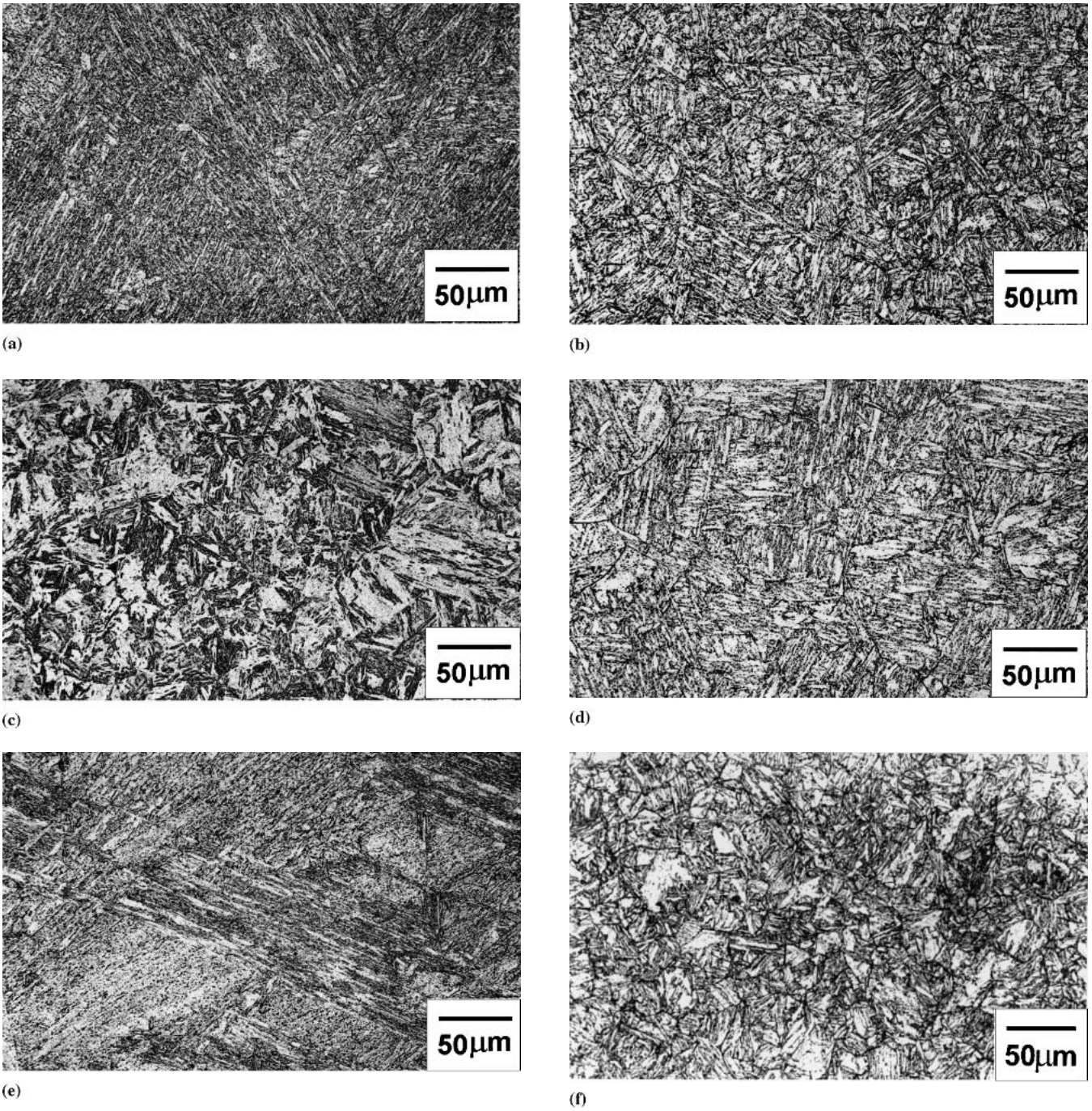

Fig. 2 Light micrographs of test materials I **(a),** J **(b),** K **(c),** L **(d),** M **(e),** and N **(f)**. Nital etch

esting to note that these excessively fragile microstructures contain, in minor or major quantity, low C martensite, whereas more ductile materials like A, J, L, and N are fully bainite microstructures. Indeed, it was realized that tempered bainite microstructures J, L, and N simulate more properly the as-irradiate state of RPV steels. Hardness and tensile testing results along with elastic plastic fracture mechanics assessments confirmed this statement.

It should be pointed out that, as likewise noticed in annealed products,[1] microstructures A, J, L, and N exhibit an inverse correlation between the reduction in area at fracture (RA), and the respective mean bainite packet size, $D_{bainite}$ (see Tables 1 and 2).

Figure 4 plots, in logarithmic scales, the relationship between RA and $D_{bainite}$, where the good data correlation is denoted by the coefficient R. Similar results obtained for annealed microstructures[1] are also provided in Fig. 4. The very close slope of the curves discloses the likeness of both thermal approaches in regard to the dependence of RA on the grain size. The notation representative cell size (RCS), will be

Table 1 Microstructural Parameters of Test Materials

Q&T Route	$D_{bainite/martensite}$, μm (a)
A (as-received)	19 (8.5)
I	775 (00)
J	105 (3.6)
K	119 (3.2)
L	153 (2.5)
M	589 (0.0)
N	25 (7.7)

(a) ASTM grain size number is provided in parentheses.

Table 2 Conventional Mechanical Properties Determined for the As-Received (A) and Thermally Embrittled Materials (I-N)

Q&T Route	BHN, 100 kgf	S_Y, MPa	S_U MPa	*n*	EL, % (a)	RA
A	175	400	555	0.15	11	77
I	340	1040	1120	0.04	10	75
J	269	725	865	0.07	07	61
K	360	970	1145	0.08	11	77
L	246	700	810	0.06	08	44
M	359	920	1195	0.14	10	70
N	212	535	700	0.12	11	73

(a) $L_0 \cong 40$ mm $\cong 10\ D_0$

adopted hereafter to refer to the significant cell size of a particular microstructure, irrespective if Q&T or annealed materials. In this regard, RCS equals the equivalent grain size (EGS), for dual-phase ferrite/bainite annealed products,[1] whereas it is $D_{bainite}$ value for single-phase tempered bainite obtained by Q&T heat treatments.

As likewise already found for annealed materials,[1] the values of RA and RCS for Q&T microstructures obey a Hall-Petch type relationship[4,5] given by the following:

$$RA = a.\ RCS^{-b} \qquad \text{(Eq 2)}$$

where *a* and *b* are fitting constants.

This power-law relationship indicates that, similarly to annealed materials,[1] RA is grain-size driven in Q&T microstructures as well. Later in this article, the same dependence will be shown regarding to their fracture toughness properties.

4.3 J-R Curves and Fracture Toughness Criteria

Figure 5 presents typical J-Δ*a* data points obtained for Q&T materials. Except for microstructures I, K, and M, which exhibited little crack propagation, extensive ductile crack growth is observed, typically in the range from 2.5-4 mm, required for the determination of J_i, J_{50}, and $dJ_D/d\Delta a_{(1\ mm)}$ criteria, as previously defined.[1]

Observe that the rank established for RA, in terms of bainite packet size (see Fig. 4), is faithfully obeyed for the J-R curves positioning, signalizing that RCS also rules the ductile crack growth resistance of Q&T materials.

By comparing Fig. 5 (a) and (b), it is verified that, as expected, a deeper SG level produces more conservative J-R curves because of higher plastic constraint, i.e., more predominant stress triaxility along the crack leading edge. Also, a slight J-specimen size dependence for the microstructure J is noticed in Fig. 5(b), with the thinner test piece giving a less-conservative J-R curve, as a consequence of loss of plastic constraint, i.e., stress relaxation along the crack front.

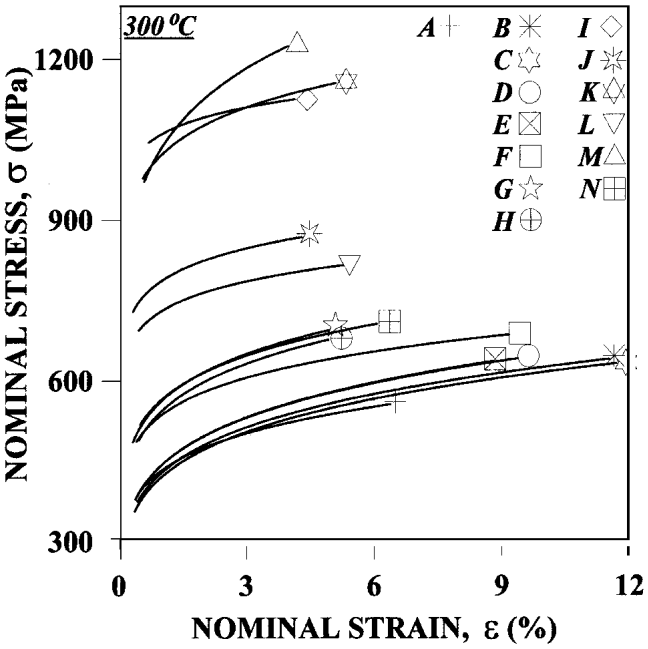

Fig. 3 Power-law stress-strain curves derived according to Eq 1. Results referring to annealed materials[1] are also included.

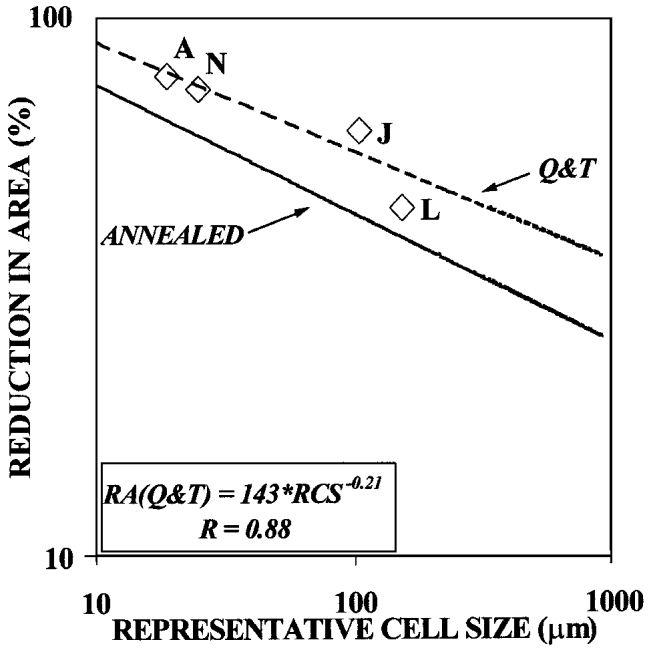

Fig. 4 Relationship between equivalent cell size and reduction in area, according to Eq 2. A baseline is drawn from results for annealed materials.[1]

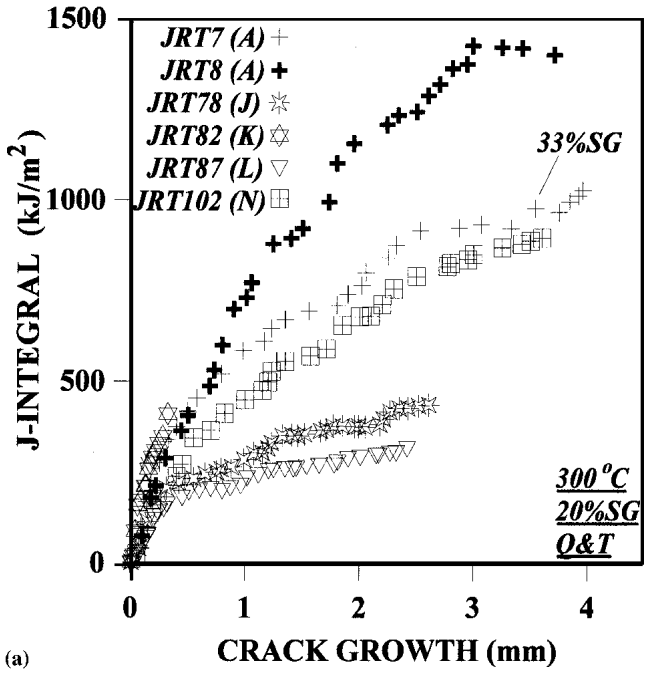

(a)

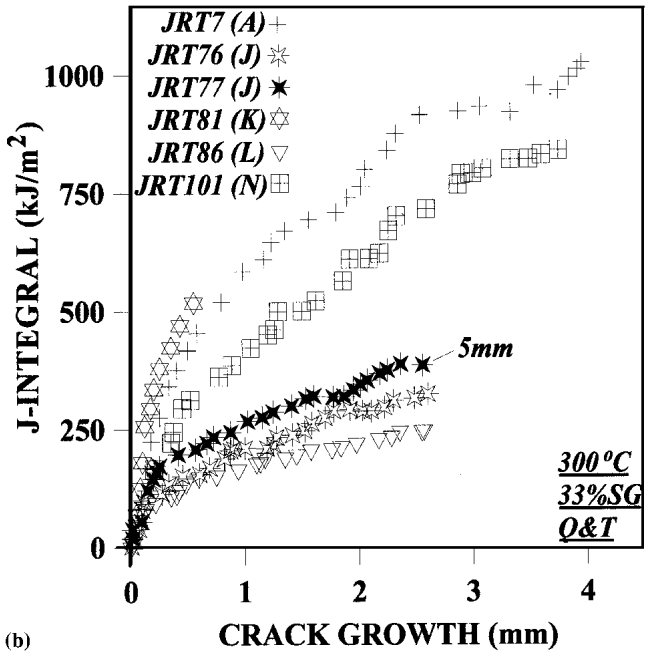

(b)

Fig. 5 Typical J-Δ*a* curves for materials tested. **(a)** 20% SG; **(b)** 33% SG test pieces. J-specimens are 10 mm thick unless otherwise indicated. J-R curves of original A508 steel are supplied as a baseline.

Given the reduced size of the test pieces, only the 10 mm thick specimens correspondent to the microstructure L fulfilled both maximum J-capacity and minimum thickness requirements to assure predominant plane-strain conditions.[6] In this case, J_i value should be quoted J_{IC}. Even though J_{IC} values could be derived for microstructure K whose J-R data are plotted in Fig. 5, the incipient ductile crack growth developed soon before the catastrophic failure of the test specimens prevented both J_{50} and $dJ_D/d\Delta a_{(1\ mm)}$ criteria from being derived. There-

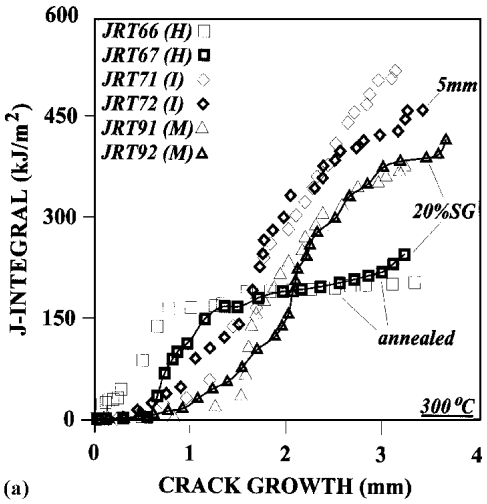

(a)

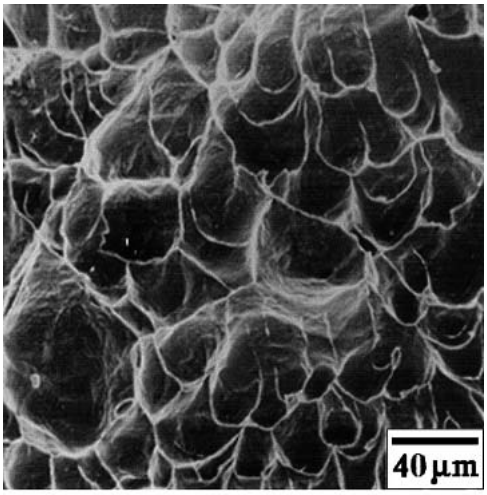

(b)

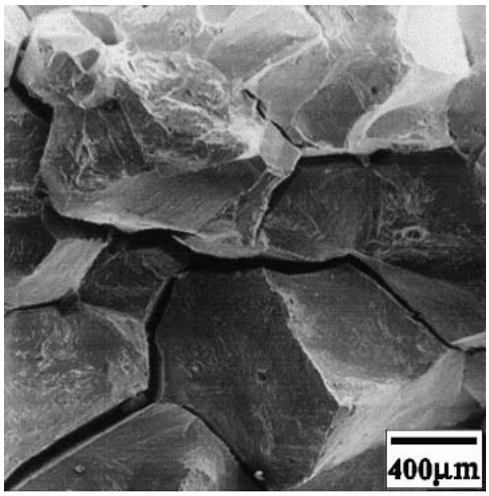

(c)

Fig. 6 **(a)** Anomalous J-R curves of unduly brittle microstructures. Test pieces are Q&T, 33%SG, and 10 mm thick unless otherwise stated; Fractographic aspects of **(b)** annealed,[1] and **(c)** Q&T microstructures

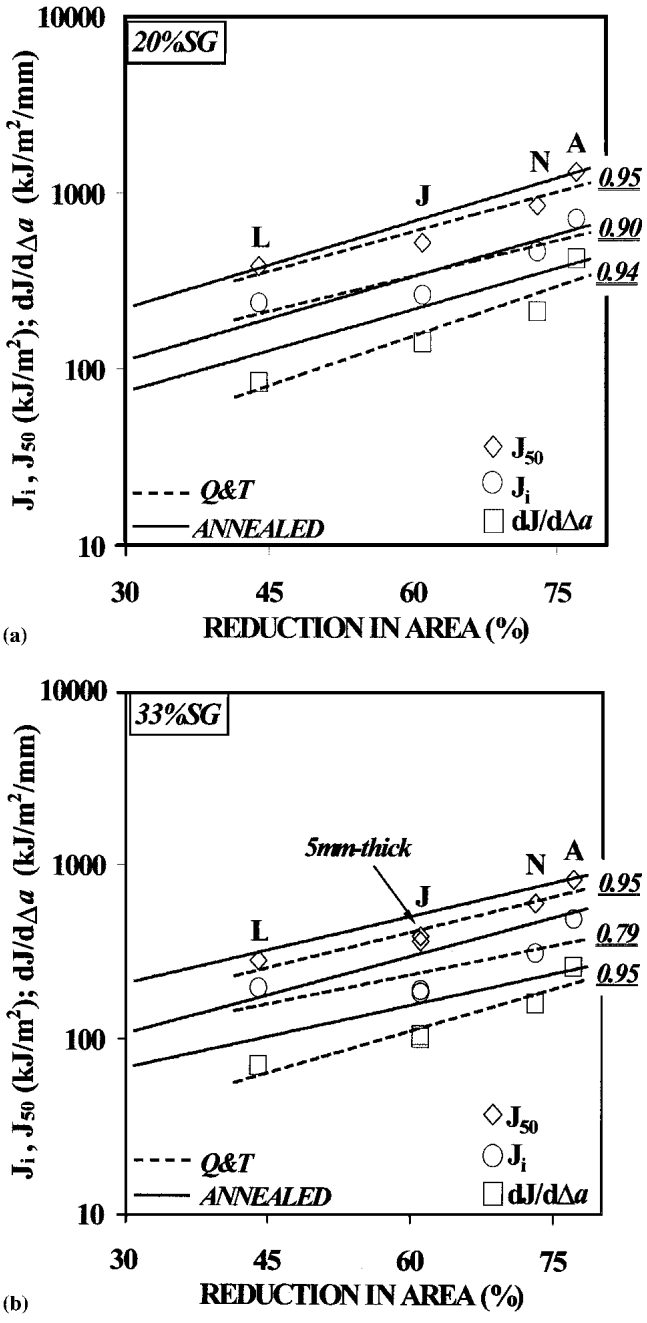

Fig. 7 Relationship between J-criteria and reduction in area, according to Eq 3. **(a)** 20% SG; **(b)** 33% SG test pieces. J-specimens are 10 mm thick unless otherwise specified. Baselines are drawn from results for annealed materials.[1]

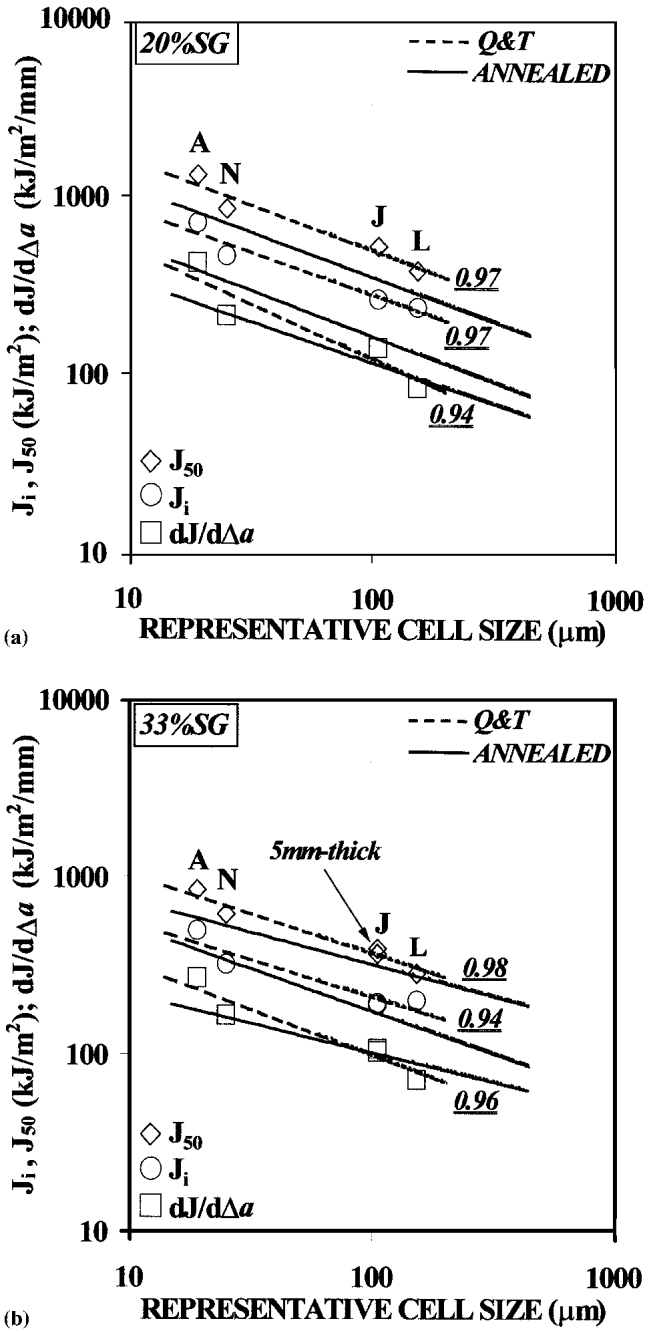

Fig. 8 Relationship between J-criteria and equivalent cell size, according to Eq 4. **(a)** 20% SG; **(b)** 33% SG test pieces. J-specimens are 10 mm thick unless otherwise noted. Baselines are drawn from results for annealed materials.[1]

fore, none of these J-criteria has been reported for that microstructure in this article.

Concerning microstructures I and M, Fig. 6(a) plots both sets of J-Δa data points, where a sigmoidal arrangement can be noticed, similar to that previously exhibited by the annealed microstructure H.[1] As earlier mentioned,[1] this behavior was probably brought about by virtue of damage accumulation at the crack tip of J-specimens during the fatigue pre-cracking step. This phenomenon caused a transgranular mode of fracture in microstructure H, Fig. 6(b), whereas an intergranular mode of rupture was observed for both microstructures I, Fig. 6(c), and M. It is speculated that manganese, and especially carbon segregation, which were massively detected by microanalysis of fracture surfaces, took place during the very high austenitizing step temperatures, so that huge final grain sizes and sigmoidal J-R curve shape have always been found closely related.

Table 3 Exponent *f* From Eq 4

Fracture Toughness Index	Heat Treatment	Exponent *f* (a) Testpiece Side-Groove Level 20% SG	33%SG
J_{50}	annealing	0.499 (−0.2)	0.425 (−15)
J_i	annealing	0.513 (+2.6)	0.480 (−4.0)
$dJ_D/d\Delta a_{(1mm)}$	annealing	0.470 (−6.0)	0.405 (−19)
J_{50}	Q&T	0.507 (+1.4)	0.467 (−6.6)
J_i	Q&T	0.478 (−4.4)	0.445 (−11)
$dJ_D/d\Delta a_{(1mm)}$	Q&T	0.590 (+18)	0.514 (+2.8)

(a) Results referring to annealed materials[1] are included.
Percentage difference in regard to the Hall-Petch exponent of 0.5 is given in parentheses.

Figure 7 shows, in logarithmic scale, the relationships between RA and J-based fracture toughness criteria, namely, J_i, J_{50}, and $dJ_D/d\Delta a_{(1mm)}$. With no exceptions, data correlation is quite encouraging. Results regarding annealed microstructures[1] are provided as a baseline. Similar to previous work,[1] J-based criteria of Q&T materials obey an exponential law regarding RA given by the following:

$$J = c.\ \exp^{(d.RA)} \quad \text{(Eq 3)}$$

where c and d are fitting constants.

The above figures establish indirectly the dependence of J-criteria with the RCS concept, as long as RA has already been proved to strongly depend on that parameter (Fig. 4). In Fig. 8, this expected dependence is shown for Q&T materials according to a Hall-Petch type relationship, which has already been shown to hold for duplex microstructures,[1] given by the following:

$$J = e.\ RCS^{-f} \quad \text{(Eq 4)}$$

where e and f are fitting constants.

Similar results obtained for annealed materials[1] are simultaneously plotted in Fig. 8. For a given value of RCS, it is observed that annealed microstructures exhibit a poorer fracture toughness performance related to Q&T. Conversely, if a constant RA value is considered in Fig. 7, a better performance is noticed for the former microstructures.

Table 3 lists the values of the exponent f in Eq 4 for Q&T and annealed materials.[1] It can be noticed that Q&T results are in very close agreement with the well-known Hall-Petch exponent value of 0.5. Although results derived for annealed materials are equally auspicious, they are hoped to even be improved by developing more sophisticated approaches in formulating the EGS concept.

5. Concluding Remarks

The elastic-plastic fracture toughness and crack extension behavior under quasi-static loading regimen of single-phase Q&T microstructures of a low alloy RPV steel were assessed on the basis of microstructural parameters. It was concluded that the grain size of the microstructures is the fracture properties controlling factor. The dependence of J-criteria on bainite packet size obeys a Hall-Petch type relationship, confirming propositions scarcely available in the literature.[7,8] It was also determined that the area reduction obtained in the tensile tests correlates fairly well to several ductile crack propagation resistance criteria. The results agree very well with trends observed in a parallel research conducted with annealed microstructures obtained from the same low alloy steel. Hence, the whole study has enlarged the possibilities of obtaining a broad range of fracture toughness for a nuclear grade steel, as a way to simulate the mechanical behavior, viz., fracture toughness of in-service neutron exposed structural materials. This procedure can lead to considerable simplification, cost and time savings, as well as risk reduction in periodic inspection programs and related subjects of nuclear industry.

Acknowledgments

The authors are grateful to FAPESP (contract 97-05652/1) for financial support.

References

1. J.R. Tarpani, W.W. Bose Filho, and D. Spinelli: "Grain Size Effects in the Quasi-Static Fracture Resistance of a Thermally Embrittled RPV Steel (Annealed Microstructures)," *Mater. Eng. Perform,* 2002, *11*(4), pp. 414-21.
2. K. Onizawa and M. Suzuki: "Correlation Among the Changes in Mechanical Properties Due to Neutron Irradiation for Pressure Vessel Steels," *ISIJ Int.*, 1997, *37*, pp. 821-28.
3. X. Mao and J. Kameda: "Small-Punch Technique for Measurement of Material Degradation of Irradiated Ferritic Alloys," *J Mater. Sci.*, 1991, *26*, pp. 2436-40.
4. N.J. Petch: "The Cleavage Strength of Polycrystals," *J. Iron Steel Inst.*, 1953, *174*, pp. 25-28.
5. E.O. Hall: "The Deformation and Ageing of Mild Steel," *Proc. Phys. Soc. B.*, 1951, *64*, pp. 747-53.
6. Anon: "Designation E1820-Standard Test Method for Measurement of Fracture Toughness" in *Annual Book of ASTM Standards*, ASTM, West Conshohocken, PA, 1999.
7. M. Srinivas, G. Malakondaiah, R.W. Armstrong, and P.R. Rao: "Ductile Fracture Toughness of Polycrystalline Armco Iron of Varying Grain Size," *Acta Metall. Mater.*, 1991, *39*, pp. 807-16.
8. M. Srinivas, G. Malakondaiah, R.W. Armstrong, and P.R. Rao: "Influence of Polycrystal Grain Size on Fracture Toughness of and Fatigue Threshold in Armco Iron," *Eng. Fract. Mech.*, 1987, *28*, pp. 561-76.